SIMULTANEOUS ALGEBRAIC RECONSTRUCTION TECHNIQUE (SART): A SUPERIOR IMPLEMENTATION OF THE ART ALGORITHM

A. H. Andersen and A. C. Kak

School of Electrical Engineering
Purdue University
W. Lafayette, IN 47907

In this paper we have discussed what appears to be a superior implementation of the Algebraic Reconstruction Technique (ART). The method is based on 1) simultaneous application of the error correction terms as computed by ART for all rays in a given projection; 2) longitudinal weighting of the correction terms back-distributed along the rays; and 3) using bilinear elements for discrete approximation to the ray integrals of a continuous image. Since this implementation generates a good reconstruction in only one iteration, it also appears to have a computational advantage over the more traditional implementation of ART. Potential applications of this implementation include image reconstruction in conjunction with ray tracing for ultrasound and microwave tomography in which the curved nature of the rays leads to a non-uniform ray density across the image.

Key words: Algebraic reconstruction; digital ray tracing; tomography; ultrasound.

1. INTRODUCTION

Although filtered backprojection algorithms are the favored choice for tomographic imaging with x-rays [18], there remains an interest in the algebraic approaches due to their potential applications for diffracting sources. When tomograhpy is attempted with ultrasound and microwaves, in a majority of applications one immediately runs into difficulties caused by refraction and diffraction. Energy propagation can no longer be modeled as occurring along straight non-bending lines. It is hoped that at least for those cases where refraction is the primary culprit, a combination of digital ray tracing and algebraic reconstruction algorithms may generate images of acceptable quality [2,19].

The algebraic approach to image reconstruction from projections consists basically of two iterative techniques: the Algebraic Reconstruction Technique (ART) and the Simultaneous Iterative Reconstruction Technique (SIRT). The first, the Algebraic Reconstruction Technique, was proposed simultaneously by Gordon, Bender, and Herman [10] and by Hounsfield [16]. It derives from a simple procedure proposed by Kacmarz [17] for solving systems of consistent linear equations. ART-type methods are sequential in nature; they implement a correction to the estimated image vector in such a way that the updated estimate will satisfy a single ray-sum equation representing a ray integral--then proceed to the next equation. SIRT-type methods [8,12] are quadratic optimization methods; in their approach they attempt to correct for errors in all ray-sum equations simultaneously. Such simultaneous methods are iterative in that they reconsider the same set of ray-sum equations ad infinitum. For ART-type as well as for SIRT-type methods, we say that one iteration is completed when each ray-sum equation in the overall system has been considered exactly once.

The particular advantages of the two types of methods appear to be mutually exclusive. ART-type methods based directly on the sequential scheme of the

Kaczmarz procedure [17] enjoy a rapid convergence in the sense of the root-mean-squared error criterion; the reconstructed images, however, exhibit a very noisy salt and pepper characteristic. SIRT-type methods, on the contrary, produce fairly smooth images but require for convergence a large number of iterations. In the ART approach, a series of smooth images can be produced when relaxation parameters are introduced; only a small fraction of the error correction term as computed by the Kaczmarz procedure is applied. In the relaxation method we loose some of the rapid convergence properties of the basic ART algorithm at the benefit of more intelligible pictures.

The problems associated with the sequential ART algorithm arise because of inconsistencies in the set of equations representing the forward process. The discrete formulation does not exactly represent the line integrals of the original continuous image function. Although the Kaczmarz procedure [17] for solving a system of consistent equations has been demonstrated to converge towards a generalized inverse [25], the resulting vector is likely to represent a very noisy looking image. This develops since satisfying a single equation may result in a very noticeable stripe along the particular ray which corresponds to that equation. Repetition of such steps for rays in different directions may result in a salt and pepper appearance of the final reconstructed images.

A significant reduction in the noise can be achieved if we apply all error correction terms for rays in a particular projection simultaneously rather than in the conventional sequential fashion. Such a procedure may at a first encounter seem like a SIRT-type algorithm, and it does enjoy some of the advantages of SIRT without suffering from its costs. However, we recall that the SIRT algorithm does not involve the concept of projections in given directions in that it is an inherently discrete approach in which all ray equations are corrected for simultaneously, regardless of the order of the equations. The proposed technique is aimed at producing a smooth image estimate after the consideration of the subset of ray-sum equations associated with a particular scan direction; SIRT, on the contrary, aims at producing smooth image estimates after each *full* iteration, i.e., after all the ray-sum equations have been considered. The rationale for the implementation derives from the formulation of ART for the reconstruction of a continuous image function [23]. At each step of the reconstruction process in the continuous formulation, the updated image estimate is formed by adding a correction image determined by back-distributing the forward projection error along a continuum of rays in the given direction. Thus, the correction to each image point is uniquely determined. For a discrete image representation in which a given image element may be involved in the forward process along several adjacent rays, the conventional sequential back-distribution procedure will invariably lead to ambiguity in the correction applied to that element -- and a noisy image update will result. The simultaneous implementation solves this ambiguity problem by defining uniquely the correction term to be applied to each image element. Thus the proposed method benefits from smoother image estimates at every step of the reconstruction procedure obviating the use of relaxation parameters. Oppenheim [20] was the first to use this projection-by-projection concept of reconstruction, although he did not attribute explicitly any significance to the noise suppression feature of this approach. Eggermont et al. [7] have discussed the convergence properties of algebraic reconstruction algorithms that partition the linear equations, as is done in the projection-by-projection method.

Furthermore, the good performance of the basic ART algorithm by the root-mean-squared error criterion has prompted us to seek the key to improved reconstructions in the set-up of the equations representing the ray integrals as well as in the reconstruction procedure itself. As the number of iterations of an algorithm increases, the continued convergence will ultimately depend on the accuracy of the discrete representation of the forward projection process. It is our belief that ART is a much more powerful technique in the reconstruction of images from projections than has been demonstrated by previous implementations.

2. APPROACH

Our ultimate objective is again the reduction of the salt and pepper noise commonly associated with ART-type reconstructions. We wish to accomplish the reconstruction in essentially one iteration (i.e., each equation is considered exactly once), without relaxation, and starting from a uniform image. Furthermore, we intend to use far fewer equations per projection than is common practice with algebraic techniques. We will use a number of equations approximately equal to the number of points in the discrete image representation; for comparison, conventional systems are overdetermined by typically a factor of four [12,14,21]. Finally, we want to maintain the basic correction strategy of ART at an overall computational cost comparable to (or possibly less than, since fewer rays are required) that for the first iteration of a conventional weighted-ART algorithm.

In our attempt to reduce the error in the approximation of the ray integrals of a smooth image by finite sums, we have abandoned the traditional pixel-basis in favor of bilinear elements. Also, for a circular reconstruction region, we have taken caution in calculating the partial weights that need to be assigned to the first and last picture elements on the individual rays, i.e., the first elements just as a ray enters the circle and the last just as it exits. With fewer rays per view and, thus, less redundancy in the system of equations, we must take some additional precautions in order to reduce the noise resulting from the inavoidable, but now presumably considerably smaller, inconsistencies with real projection data. We have found that a simultaneous application of the correction terms for the rays in a particular view is preferable to the usual sequential fashion. In addition, we have used a heuristic procedure to improve the quality of reconstructions: a longitudinal Hamming window is used to emphasize the corrections applied near the middle of a ray relative to those applied near its ends.

We will proceed to describe in more detail the individual steps comprising our proposed implementation of the algebraic reconstruction technique in image reconstruction from projections. The contribution that each step makes in improving the overall accuracy of the proposed procedure will be illustrated with reconstructions of the head phantom proposed by Shepp and Logan [21]. The reconstructions on a 128×128 sampling lattice are carried out for 100 projections of 127 rays each. It should be pointed out that no "waterbag" is assumed to enclose the phantom. The waterbag is a carry-over from the initial work of Hounsfield [16] and has been assumed in most reconstructions of simulated head phantoms using ART-type algorithms [14,16,21]--it permits that, except for the skull, a uniform image as a first estimate will be in fact a very good approximation to the correct image.

3. MODELING THE FORWARD PROJECTION PROCESS

In any kind of image processing by computer we must have a way of describing pictures $f(x,y)$ by finite sets of numbers. The common approach is an expansion of a continuous image into a linear combination of N basis pictures $\{b_i(x,y)\}$ [12,13]. Thus, for any picture $f(x,y)$ there exist real numbers $g_1, g_2, \ldots, g_N$ such that

$$f(x,y) \simeq \hat{f}(x,y) \equiv \sum_{i=1}^{N} g_i \, b_i(x,y). \qquad (1)$$

$\hat{f}(x,y)$ gives an adequate approximation to the picture $f(x,y)$, and the g_i's form the finite set of numbers which describes the picture relative to the chosen basis set $\{b_i(x,y)\}$.

If $r_j(x,y) = 0$ is the equation of the j'th ray, the projection operator R_j along that ray can be expressed as

$$p_j = R_j f(x,y) = \int\limits_{-\infty}^{\infty} \int\limits_{-\infty}^{\infty} f(x,y)\delta(r_j(x,y))dxdy. \qquad (2)$$

We have assumed that $f(x,y)$ is a square integrable function which vanishes outside the unit circle. With the finite-dimensional image model, the linearity of the projection operator ensures that we have

$$R_j \hat{f}(x,y) = \sum_{i=1}^{N} g_i R_j b_i(x,y). \tag{3}$$

In practical implementations, we may want to replace the numbers $R_j b_i(x,y)$ by some approximations a_{ij} in order to facilitate computation. Thus, we obtain

$$p_j = R_j f(x,y) \simeq R_j \hat{f}(x,y) = \sum_{i=1}^{N} g_i R_j b_i(x,y) \simeq \sum_{i=1}^{N} g_i a_{ij}. \tag{4}$$

If e_j represents the error inherent in the finite-dimensional representation of the forward process, we have

$$p_j = \sum_{i=1}^{N} g_i a_{ij} + e_j. \tag{5}$$

In matrix notation we write

$$\vec{p} = [A]^T \vec{g} + \vec{e}, \tag{6}$$

where $[A]^T$ is the $J \times N$ projection matrix of the coefficients a_{ij}, and $\vec{p}$ and $\vec{e}$ are J-dimensional column vectors. The N-dimensional vector $\vec{g}$ is commonly referred to as the image vector.

In the selection of a set of basis pictures, most researchers have found the pixel basis the simplest to deal with [6,8-10,12-16,20,21]. To obtain this set we divide the square of side 2 into N identical subsquares referred to as pixels and identified by the index i, for $1 \leq i \leq N$. The basis functions become

$$b_i(x,y) = \begin{cases} 1, & \text{inside the } i\text{'th pixel} \\ 0, & \text{everywhere else} \end{cases}. \tag{7}$$

For this basis, $R_j b_i(x,y)$ exactly represents the length of the intersection of the j'th ray with the i'th pixel. If the projection matrix $[A]^T$ were computed this way, no error would be committed in the model of the forward projection process beyond that inherent in the equations from the choice of basis functions. Although Eq. (2) implies rays of zero width, if we now associate a finite width with each ray, the elements of the projection matrix will represent the areas of intersection of these ray strips with the pixels. In the original version of the ART algorithm [10], for computational ease binary coefficients were chosen for the projection matrix: a_{ij} was set equal to 1 if the center of the i'th pixel fell within the strip of the j'th ray, and 0 if not. With the representation of rays as strips of finite width, it is necessary to adjust the width of each ray according to the orientation of the projection [9,15,20].

In practically all work with ART-type algorithms, researchers have adhered to this choice of model. Higher-order basis functions have been judged too costly in computation time. One measure to combat the salt and pepper noise inherent to ART-type reconstructions with this model has been to increase the number of rays per view [22]. When the number of rays per view is increased, many pixels are intersected by several rays in each projection. This results in the averaging of possible errors committed in the correction procedure. It appears common practice to have a system with about four times as many equations as unknown pixel values [12,14,21].

The computational cost, however, is increased directly with the number of rays processed. An additional method has been to use a relaxation factor $\lambda < 1$ [9,12-14,16,24] which, although reducing the salt and pepper noise, increases the number of iterations required for convergence. Underrelaxation is now presented as the definitive technique that allows us to obtain fair reconstructions for ART with real projection data, not just with pseudo-projection data [12,13].

It is our opinion that one of the keys to improved reconstructions lies in a more accurate depiction of the forward projection process. The bilinear elements are the simplest higher-order elements [1,13]. They are "pyramid"-shaped, each with a support extending over a square region the size of four pixels. The g_i's appearing in Eq. (1) will be the sample values of the image function $f(x,y)$ on a square lattice. Whereas the pixel basis leads to a discontinuous image representation, the bilinear elements allow a continuous form while we maintain a relative ease in computation. Finding the exact ray integrals across such bilinear elements for a large number of rays is nevertheless a time consuming task and we will use an approximation.

Rather than try to find separately the individual coefficients a_{ij} for a particular ray, we opt to approximate the overall ray integral $R_j f(x,y)$ by a finite sum involving a set of M_j equi-distant points $\{\hat{f}(s_{jm})\}$, for $1 \leq m \leq M_j$ [4,19] (see Fig. 1):

$$p_j \simeq \sum_{m=1}^{M_j} \hat{f}(s_{jm}) \Delta s. \tag{8}$$

This approach was inspired by our work in ray tracing [1]. According to the chosen image representation, the value $\hat{f}(s_{jm})$ is determined from the values g_i of $f(x,y)$ on the four neighboring points of the sampling lattice, i.e., by bilinear interpolation. We write

$$\hat{f}(s_{jm}) = \sum_{i=1}^{N} d_{ijm} g_i , \quad \text{for} \quad m = 1,2,....,M_j. \tag{9}$$

Combining Eqs. (8) and (9), we obtain an approximation to the ray integral p_j as a linear function of the image samples g_i

$$p_j = \sum_{m=1}^{M_j} \sum_{i=1}^{N} d_{ijm} g_i \Delta s$$
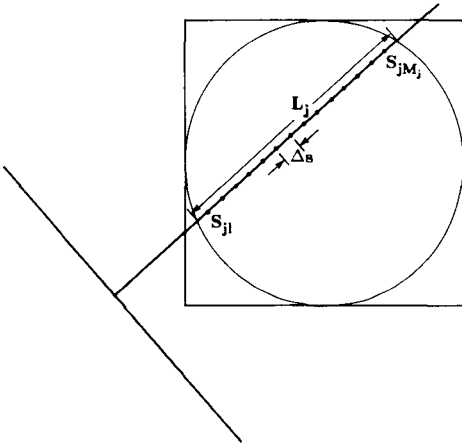

Fig. 1   Illustrating the ray-sum equations for a set of equidistant points along a straight line cut by the circular reconstruction region.

$$= \sum_{i=1}^{N} \sum_{m=1}^{M_j} d_{ijm} g_i \Delta s \qquad \text{for } 1 \leq j \leq J$$

$$= \sum_{i=1}^{N} a_{ij} g_i \quad , \tag{10}$$

where the coefficients a_{ij} represent the net effect of the linear transformations. They are determined as the sum of the contributions from different points along the ray

$$a_{ij} = \sum_{m=1}^{M_j} d_{ijm} \Delta s. \tag{11}$$

It is important to the overall accuracy of the model that for $m=1$ and for $m=M_j$, i.e., for the first and last points of the ray within the reconstruction circle, the weights are adjusted so that $\sum_{i=1}^{N} a_{ij}$ equals the actual physical length L_j.

In the choice of step-size Δs, we have found that setting it equal to half the spacing of the sampling lattice provides a good trade-off between accuracy of representation and computational cost. For this choice of step length, it is our judgement that, considering the computational simplicity of finding the weights d_{ijm} associated with a bilinear interpolation, the overall cost of finding the net effects a_{ij} this way should be comparable to the cost involved in finding the a_{ij}'s as intersections with the pixels in the traditional formulation.

4. IMPLEMENTATION OF THE RECONSTRUCTION ALGORITHM

Our computer simulation results will be shown for the image of figure 2a. This is the well known Shepp and Logan [21] "head phantom", which consists of a number of ellipses of varying sizes and densities. [The advantage of using ellipses is
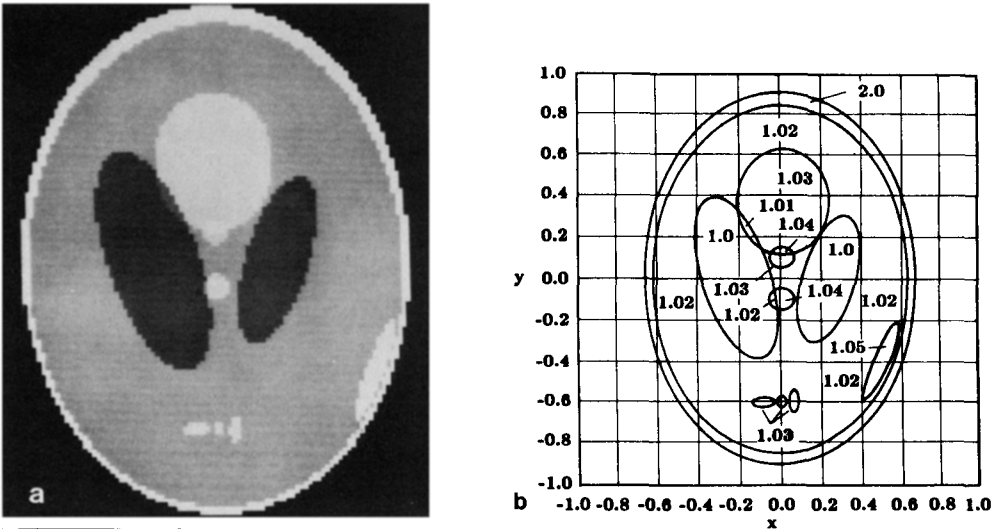

Fig. 2   (a) Illustrating the Shepp and Logan head phantom with a subdural hematoma. (b) The gray level distribution of the Shepp and Logan phantom is shown here.

that one can write mathematical expressions for their projections, and therefore the "real" projection data for the image of figure 2a can be generated by summing the line integrals for individual ellipses thus obtained.] The gray level distribution in the test image is shown in figure 2b.

Using this procedure, we analytically determine the line integral data for the test image for 127 rays in each of 100 projections, and the image is reconstructed on a 128×128 sampling lattice. In the model of Eq. (10), this corresponds to $N = 16384$ picture elements and an overall number of rays $J = 12700$. We notice that the system of equations is underdetermined by about 25 percent, but then the reconstruction circle covers only about 75 percent of the area of the square sampling lattice. Reconstructions from this data will be shown without assuming the existence of the "waterbag" around the head phantom. Thus, ours becomes a much more difficult task than the reconstructions shown with the waterbag [14,21] where a uniform density of 1.0 as a first estimate is indeed a very good approximation to the correct image.

The error-correcting procedure of the basic sequential ART algorithm [9,10,12-16] can be written as

$$\vec{g}^{(k+1)} = \vec{g}^{(k)} + \vec{a}_j \frac{p_j - \vec{a}_j^T \vec{g}^{(k)}}{\vec{a}_j^T \vec{a}_j} \; , \tag{12}$$

where $\vec{a}_j$ denotes the j'th column vector of the matrix $[A]$. The estimate $\vec{g}^{(k)}$ of the image vector is updated after each ray has been considered. The initial estimate $\vec{g}^{(0)}$ is set to a uniform image of zero density. We say that one iteration of the algebraic reconstruction technique is completed when all J rays, i.e., all J ray-sum equations, have been used exactly once. In order to efficiently use the information in the system of Eqs. (10), we consider projections taken at angles far apart (in our implementation 73.8 °). This procedure was introduced by Hounsfield [16] based on an heuristic argument as to the high correlation between the information in neighboring projections. Later the scheme was demonstrated to have a deeper mathematical foundation as a tool for speeding up the convergence of ART-type algorithms. (The proof relies on a continuous formulation of ART, as shown by Hamaker and Solmon [11].)

Figure 3a illustrates the reconstruction of the head phantom for one iteration of the conventional sequential ART algorithm. In order to avoid streak artifacts in the final image, the correction terms for the first few projections were deemphasized relative to those of projections considered later on . The image has been thresholded to the density interval .95-1.05 to illustrate the finer detail. We notice that even the larger structures are buried in the salt and pepper noise present when no form of relaxation or smoothing is used. Figure 3b shows a line plot through the three small tumors of the phantom (we have plotted the profile along the line $y = -.605$). We observe that the amplitude variations of the noise largely exceed the density differences characterizing these structures.

Figure 4a illustrates the reconstruction when a simultaneous application of all correction terms for a given scan direction is used. In this implementation, we compute the individual correction terms in the usual fashion. The terms are then saved until all rays in that view have been considered. The average correction to each picture element is computed and added to form the updated image:

$$g_i^{(k+1)} = g_i^{(k)} + \frac{\sum_j \left[a_{ij} \dfrac{p_j - \vec{a}_j^T \vec{g}^{(k)}}{\sum_{i=1}^{N} a_{ij}} \right]}{\sum_j a_{ij}} \; , \tag{13}$$
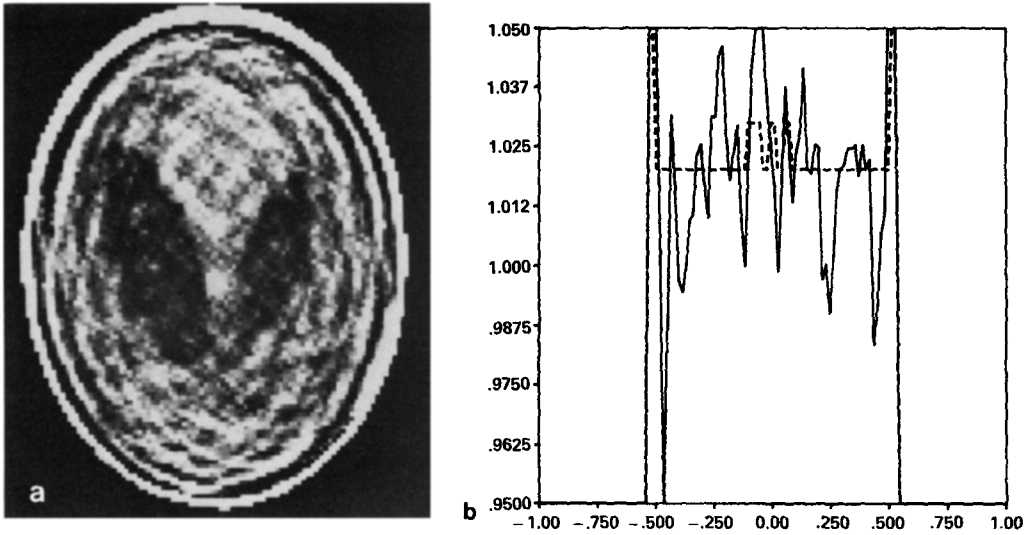
Fig. 3   Reconstruction from one iteration of sequential ART (a) Image (b) Line plot through the three small tumors (for $y = -.605$).

where the summation with respect to j is over the rays intersecting the ith image element for a given scan direction. The factor $\sum\limits_{i=1}^{N} a_{ij}$ in the denominator of the individual correction terms (the term in the square bracket) equals the actual physical length L_j of the jth ray. The replacement of $\vec{a}_j^T \vec{a}_j$ by $\sum\limits_{i=1}^{N} a_{ij}$ in the simultaneous procedure is done for reasons of uniformity of the reconstructed image. Furthermore, it maintains the correct dimensions for the updated image vector.
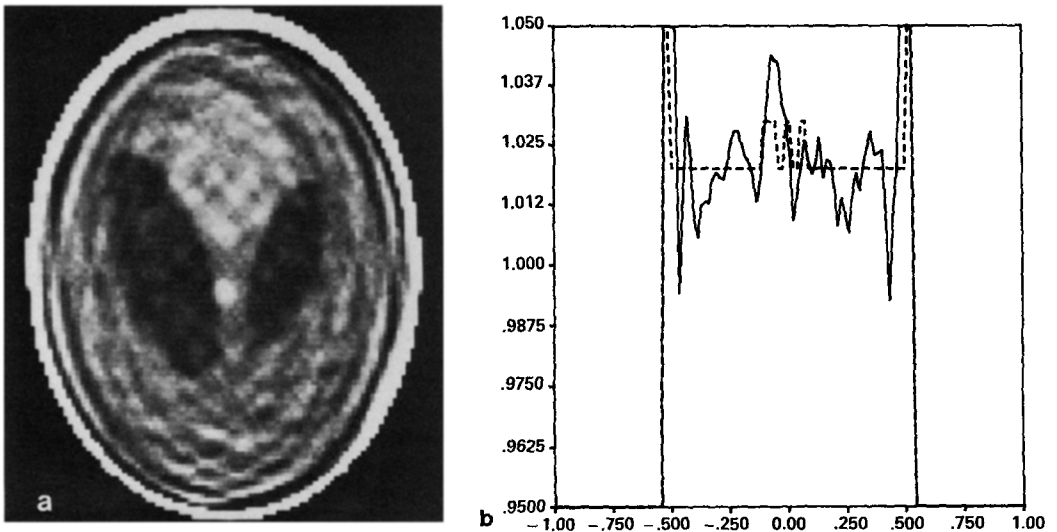

Fig. 4   Reconstruction from one iteration of simultaneous ART (a) Image (b) Line plot through the three small tumors (for $y = -.605$).

A simplified form of the simultaneous technique was used by Oppenheim in [20]. However, the scope of the implementation as described by Eq. (13) is much wider. The method can be used advantageously in the general image reconstruction problem for curved rays with overlapping and non-onverlapping ray strips as well as in conjunction with any image representation, provided the forward process can be expressed in the form of Eq. (4).

Compared to the reconstruction of figure 3 for the sequential scheme, the simultaneous method offers a reduction in the amplitude of the noise. In addition, the noise in the reconstructed image has become more slowly undulating compared to the previous salt and pepper appearance. This technique maintains the rapid convergence of ART-type algorithms while at the same time it has the noise suppressing features of SIRT [8]. As with SIRT, our simultaneous implementation does require the storage of an additional array for the correction terms. The simultaneous procedure is justified by the argument that the corrections from all rays in a particular view should result in a continuous image function [23].

We will now present a heuristic procedure that has not previously been used in conjunction with ART algorithms. We will modify the back-distribution of the correction terms by a longitudinal Hamming window. The idea of the window is illustrated in figure 5. The conventional, basically uniform back-distribution according to the coefficients a_{ij} is replaced by a weighted version. This corresponds to replacing the standard correction term

$$\vec{a}_j \frac{p_j - \vec{a}_j^T \vec{g}^{(k)}}{\sum_{i=1}^{N} a_{ij}} \tag{14}$$

by a weighted correction term

$$\vec{w}_j \frac{p_j - \vec{a}_j^T \vec{g}^{(k)}}{\sum_{i=1}^{N} a_{ij}} \tag{15}$$

where the weighting coefficients w_{ij} are determined as (compare with Eq. (11))

$$w_{ij} = \sum_{m=1}^{M_j} h_{jm} d_{ijm} \Delta s. \tag{16}$$
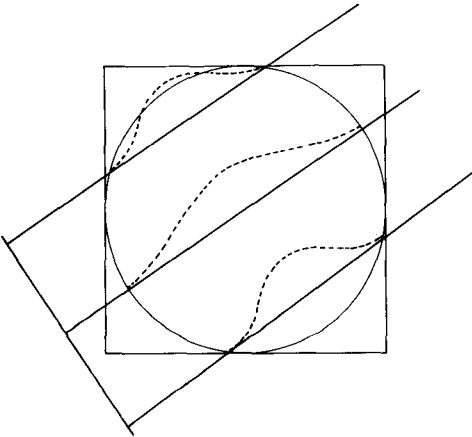

Fig. 5   Illustrating the longitudinal Hamming window for a set of straight rays.
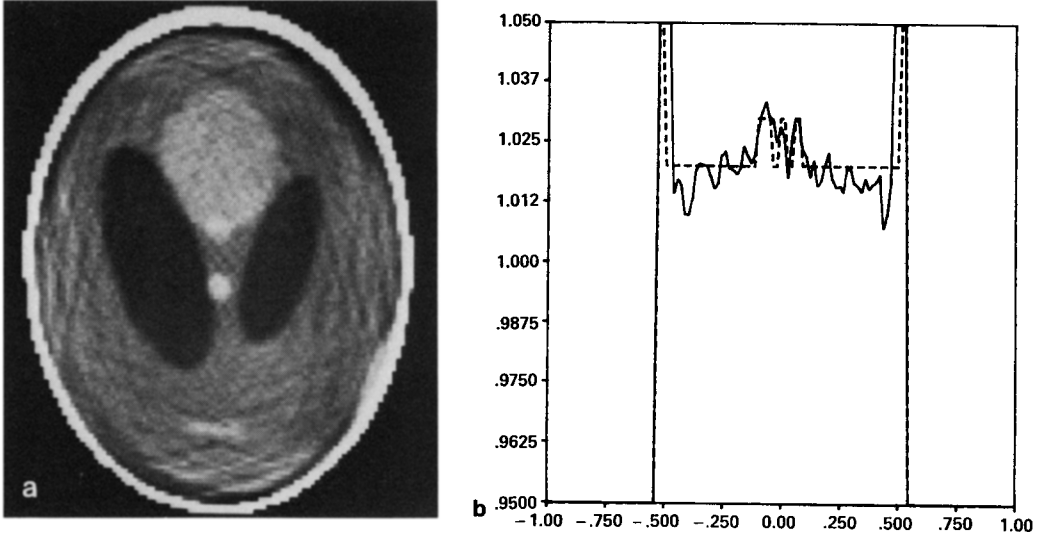
Fig. 6   Reconstruction from one iteration of simultaneous ART with a longitudinal
Hamming window (a) Image (b) Line plot through the three small tumors
(for $y = -.605$).

The sequence h_{j_m}, for $1 \leq m \leq M_j$, is a Hamming window of length M_j. We notice
that the length of the window varies according to the number of points M_j describ-
ing the part of the ray cut by the reconstruction circle. The basic difference between
Eqs. (14) and (15) lies in the first factor. The denominator in both cases is the same.
If we change the denominator from $\sum\limits_{i=1}^{N} a_{ij}$ to $\sum\limits_{i=1}^{N} w_{ij}$, the discontinuous jumps in
$\sum\limits_{i=1}^{N} w_{ij}$ (caused by the discretized length of the window) will result in edges after the
correction from a single projection and salt and pepper noise in the final image. The
use of this "filter" will require the storage of an additional array to hold the
coefficients w_{ij}.

The incorporation of the longitudinal Hamming window has an intuitive appeal
in that objects are most often of a convex shape and located centrally within the
reconstruction circle. The back-distribution procedure should therefore emphasize
central portions of the rays to distal portions. Figure 6 illustrates a reconstruction
of the head phantom after one iteration with the longitudinal window in conjunction
with the simultaneous scheme previously described. We see an amazing improve-
ment from the reconstructions of figures 3 and 4: the noise is practically gone and
the structures within the skull including the hematoma can be fairly well dis-
tinguished. The longitudinal Hamming window has proven to be a most powerful
step in suppressing noise, and giving a contrast enhancement at the same time. If
we had not applied the corrections in a simultaneous scheme but incorporated the
longitudinal Hamming window only for the conventional sequential implementation,
we would have arrived at the noisy reconstruction illustrated in figure 7. Based on
the reconstructed image of figure 6, further iterations as illustrated by figures 8 and
9 bring out even more contrast at a cost, though, of a beginning appearance of salt
and pepper noise. The subdural hematoma can now be clearly distinguished. All
reconstructions shown represent the raw output from the algorithms with no post-
processing applied to suppress noise.

For the purpose of comparison, we have included in figure 10 the resulting
image using the technique of convolution back-projection. The reconstructions with
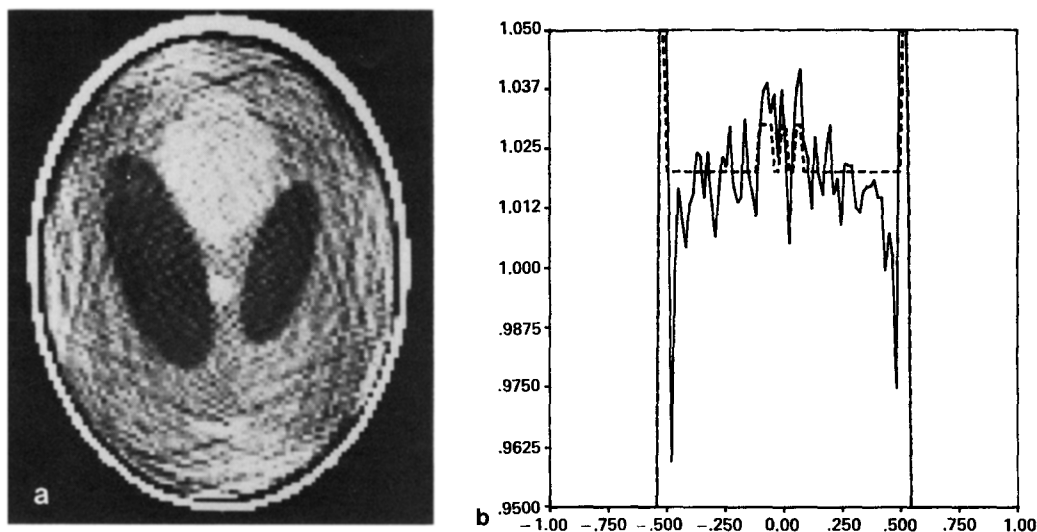
Fig. 7   Reconstruction from one iteration of sequential ART with a longitudinal Hamming window (a) Image (b) Line plot through the three small tumors (for $y = -.605$).

our implementation of the algebraic reconstruction technique are of a quality, that at least from a numerical standpoint, is essentially what is obtained with convolution back-projection. With regard to this conclusion, the reader may wonder about the noise that is so apparent in the photo in figure 9 and those preceding it. Note from the plots shown below the reconstruction, the noise in figure 9 represents a maximal deviation of only about 0.5 percent.
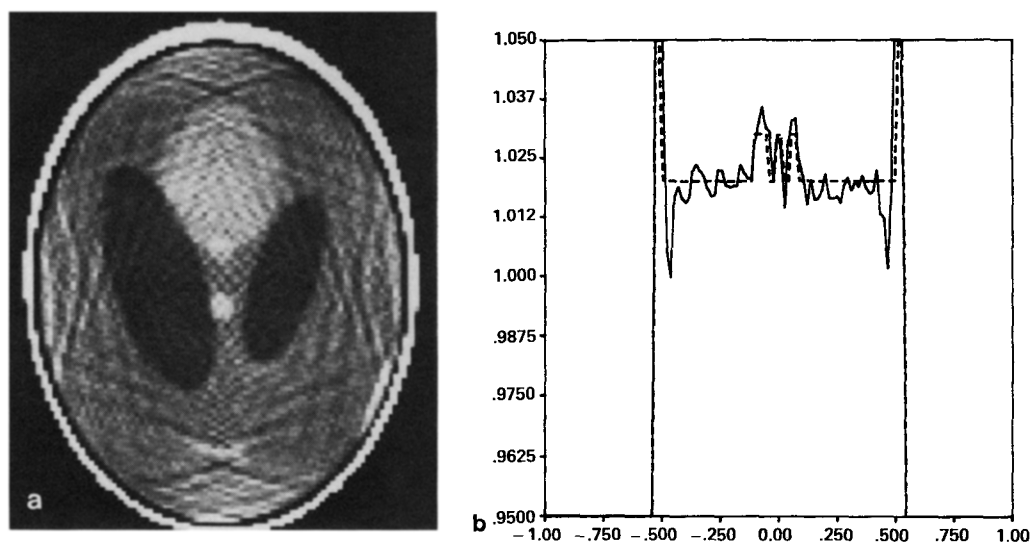

Fig. 8   Reconstruction from two iterations of simultaneous ART with a longitudinal Hamming window (a) Image (b) Line plot through the three small tumors (for $y = -.605$).
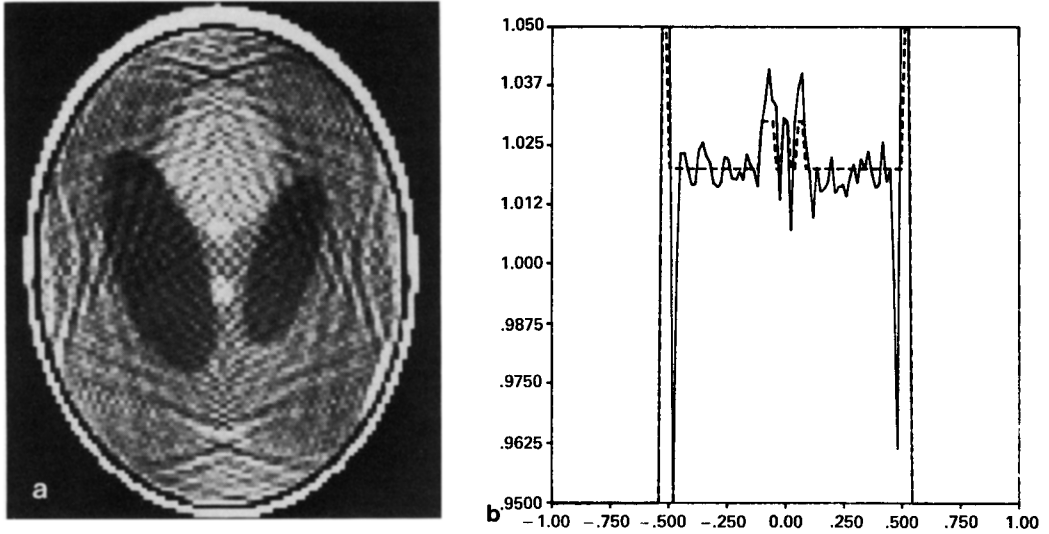
Fig. 9   Reconstruction from three iterations of simultaneous ART with a longitudinal Hamming window (a) Image (b) Line plot through the three small tumors (for $y = -.605$).

5. CONCLUSION

We have presented significantly improved reconstructions in fewer iterations (essentially just one iteration) with fewer rays per iteration and in a simple simultaneous implementation of the ART algorithm. We will leave it up to the individual reader to decide for him/herself which reconstruction is the most pleasing. To us the reconstructed image after the first iteration appears to suffer least from the effects of noise, whereas the line plot after the second iteration is the one closest to the correct
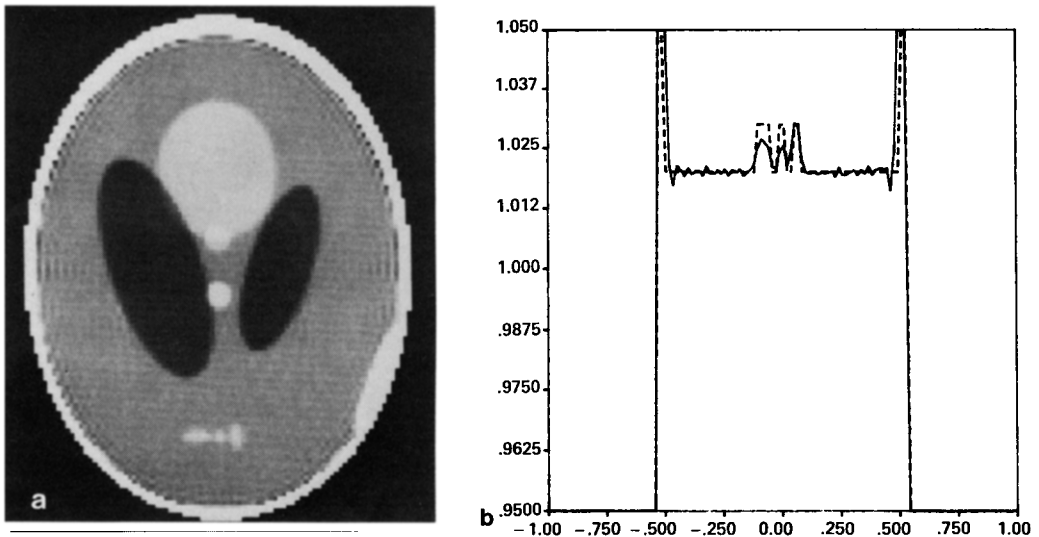

Fig. 10   Convolution back-projection reconstruction of the head phantom (a) Image (b) Line plot through the three small tumors (for $y = -.605$).

profile. However, we can say that the increased amplitude of the salt and pepper noise pattern with an increase in the number of iterations is an indication of remaining inconsistencies in our model of the forward projection process.

A potential application of the Simultaneous Algebraic Reconstruction Technique lies in the reconstruction along curved rays for ultrasound and microwave tomography in which case the ray density is non-uniform across an image. This non-uniformity in conjunction with a conventional sequential implementation leads to unacceptable spurious effects. Curved-ray reconstruction algorithms with single-iteration convergence are expected to be of considerable value to the ongoing work in ultrasonic transmission tomography. While addressing some of the degradations associated with refraction effects [3], this work has hitherto been based on the assumption of straight-ray propagation.

ACKNOWLEDGEMENT

REFERENCES

[1] Andersen, A. H. and Kak, A. C., Digital ray tracing in two-dimensional refractive fields, *J. Acoust. Soc. Am.* *72*, 1593-1606, (1982).

[2] Cha, S. and Vest, C. M., Tomographic reconstruction of strongly refracting fields and its application to interferometric measurements of boundary layers, *Applied Optics* *20*, 2787-2794, (1981).

[3] Crawford, C. R. and Kak, A. C., Multipath artifact corrections in ultrasonic transmission tomography, *Ultrasonic Imaging* *4*, 234-266, (1982).

[4] Crowther, R. A., DeRosier, D. J. and Klug, A., The reconstruction of a three-dimensional structure from projections and its application to electron microscopy, *Proc. Royal Soc. London* *A317* 319-340 (1970).

[5] Crowther, R. A. and Klug, A., Three dimensional image reconstruction on an extended field--a fast, stable algorithm, *Nature* *251*, 490-492 (1974).

[6] Dines, K. A. and Lytle, R. J., Computerized geophysical tomography, *Proc. IEEE*, *67*, 1065-1073 (July 1979).

[7] Eggermont, P. P. B., Herman, G. T. and Lent, A., Iterative algorithms for large partitioned linear systems with applications to image reconstruction, *Linear Algebra and its Applications* *40*, 37-67, (1981).

[8] Gilbert, P., Iterative methods for the three-dimensional reconstruction of an object from projections, *J. Theor. Biol.* *36*, 105-117 (1972).

[9] Gordon, R., A tutorial on ART (Algebraic Reconstruction Techniques), *IEEE Trans. Nucl. Sci.* *NS-21*, 78-93 (1974).

[10] Gordon, R., Bender, R. and Herman, G. T., Algebraic Reconstruction Techniques (ART) for three-dimensional electron microscopy and x-ray photography, *J. Theor. Biol.* *29*, 471-481 (1970).

[11] Hamaker, C. and Solmon, D. C., The angles between the null spaces of X rays, *J. Math. Anal. Appl.* *62*, 1-23 (1978).

[12] Herman, G. T., *Image Reconstruction from Projections: The Fundamentals of Computerized Tomography*, (Academic Press, New York, 1980).

[13] Herman, G. T. and Lent, A., Iterative Reconstruction algorithms, *Comput. Biol. Med.* *6*, 273-294 (1976).

[14] Herman, G. T., Lent, A. and Lutz, P. H., Relaxation methods for image reconstruction, *Comm. A. C. M.* *21*, 152-158 (1978).

[15] Herman, G. T., Lent, A. and Rowland, S., ART: mathematics and applications, *J. Theor. Biol.* *42*, 1-32 (1973).

[16] Hounsfield, G. N., A method and apparatus for examination of a body by radiation such as X or Gamma radiation, Patent Specification 1283915, London, England (1972).

[17] Kaczmarz, S., Angenaherte auflosung von systemen lenearer gleichungen, *Bull. Int. Acad. Pol. Sci. Lett. A.*, 355-357 (1937)..

[18] Kak, A. C., Computerized tomography with X-ray, emission, and ultrasound sources, *Proc. IEEE 67*, 1245-1272 (1979).

[19] Lytle, R. J. and Dines, K. A., Iterative ray tracing between boreholes for underground image reconstruction, *IEEE Trans. Geos. Remote Sensing GE-18*, 234-240 (1980).

[20] Oppenheim, B. E., Reconstruction tomography from incomplete projections, in *Reconstruction Tomography in Diagnostic Radiology and Nuclear Medicine*, M. M. Ter-Pogossian et al., eds. (University Park Press, 1977).

[21] Shepp, L. A. and Logan, B. F., The Fourier reconstruction of a head section, *IEEE Trans. Nucl. Sci. NS-21*, 21-43 (1974).

[22] Smith, K. T., Solmon, D. C. and Wagner, S. L., Practical and mathematical aspects of the problem of reconstructing objects from radiographs, *Bull. Am. Math. Soc.* *83*, 1227-1270 (1977).

[23] Solmon, D. C., The X-ray transform, *J. Math. Anal. Appl.* *56*, 61-83 (1976).

[24] Sweeney, D. W. and Vest, C. M., Reconstruction of three-dimensional refractive index fields from multi-direction interferometric data, *Appl. Opt.* *12*, 2649-2664 (1973).

[25] Tanabe, K., Projection method for solving a singular system of linear equations and its applications, *Numer. Math.*, 203-214 (1971).